crystals

MDPI

Article

Lyotropic Liquid Crystal System for Drug Delivery of Astaxanthin: Physical Characterization and Enhanced Antioxidant Potential

Sapna Kumari [1], Anju Goyal [1,*], Madhukar Garg [1], Angela Antonescu [2] and Rakesh K. Sindhu [3,*]

[1] Chitkara College of Pharmacy, Chitkara University, Punjab 140401, India
[2] Faculty of Medicine and Pharmacy, University of Oradea, Pta 1 Decembrie 10, 410087 Oradea, Romania
[3] School of Pharmacy, Sharda University, Greater Noida, Uttar Pradesh 201310, India
* Correspondence: anju.goyal@chitkara.edu.in (A.G.); rakeshsindhu16@gmail.com (R.K.S.)

Abstract: Astaxanthin is a xanthophyll carotenoid, well known for its potent anti-inflammatory and antioxidant properties, owing to its unsaturated molecular structure. Aquatic plants and animals contain the hydrophobic carotenoid astaxanthin, which is thought to possess a number of advantageous biological traits. However, due to its weak bioavailability and low water solubility, its use as a nutraceutical in food is currently restricted. Cubosomal encapsulation has been considered an effective alternative for improving the bioavailability and solubility of hydrophobic bioactives. The current paper aimed to conquer these issues by encapsulating astaxanthin in lyotropic liquid crystal nano-formulations prepared via the fabrication method. The physicochemical properties of astaxanthin-loaded cubosomes (AST-LC) have also been analyzed, in order to know the morphology of the prepared formulations and their bioavailability in the biological system. The formulation has been tested for particle size, thermal behavior, zeta potential, crystallinity, encapsulation efficiency, and drug-polymer interactions. The observed experimental results showed the particle size and zeta potential of astaxanthin-loaded cubosomes (AST-LC) as 199 $\pm$ 0.23 nm $-$27.4 $\pm$ 4.67 mV, with a small polydispersity index (0.283 $\pm$ 1.01). The cubic structure and nano-range size of the ideal formulation were verified by a field emission scanning electron microscope (FESEM) and (HRTEM) high-resolution transmission electron microscopic examination. The formulation exhibits a higher encapsulation efficiency with good yield. Results from X-ray diffraction and diffraction scanning calorimetry demonstrated an amorphous state of astaxanthin incorporated into the formulation. Fourier transform infrared spectroscopy (FTIR) analysis of AST-LC showed the absence of astaxanthin main peaks, indicating its complete encapsulation inside the formulation. The drug–excipient interaction was carried out with diffraction scanning calorimetry DSC and FTIR, resulting in no interaction between them. These results offered important details about increasing astaxanthin bioavailability by incorporating it into cubosomes. Furthermore, the astaxanthin loaded into cubosomes has been evaluated for antioxidant potency, compared with astaxanthin extract using 2,2-diphenylpicrylhydrazylassay (DPPH assay).

Keywords: astaxanthin; cubosomes; antioxidant; poloxamer 407; GMO

Citation: Kumari, S.; Goyal, A.; Garg, M.; Antonescu, A.; Sindhu, R.K. Lyotropic Liquid Crystal System for Drug Delivery of Astaxanthin: Physical Characterization and Enhanced Antioxidant Potential. *Crystals* **2023**, *13*, 142. https://doi.org/10.3390/cryst13010142

Academic Editors: Mohammed Rafi Shaik, Syed Farooq Adil and Mujeeb Khan

Received: 2 December 2022
Revised: 28 December 2022
Accepted: 29 December 2022
Published: 13 January 2023

1. Introduction

A carotenoid called astaxanthin is present in many marine plants and animals, including algae [1]. Numerous studies have demonstrated the therapeutic benefits of astaxanthin, including its ability to prevent cancer, reduce inflammation, protect skin from UV damage, and slow the progression of age-related macular degeneration [2,3]. Although astaxanthin is a potent antioxidant, its higher lipophilicity and low water solubility has limited its oral bioavailability. Due to its ability to neutralize singlet oxygen, free radicals, and prevent lipid peroxidation in biological membranes, astaxanthin is frequently utilized as a nutritional supplement and cosmetic element [4]. Recently, astaxanthin has gained a lot of attention,

owing to its higher antioxidant activity when compared with beta-carotene, vitamin E, and coenzyme Q10 [5,6]. However, its exceptionally low water solubility and poor oral bioavailability limit its use as a nutraceutical in foods, supplements, and other commercial items. Additionally, sometimes a loss in the antioxidant potential occurs due to a chemical breakdown during processing, storage, and digestion. Astaxanthin degrades when exposed to acidic pH conditions, specific enzymes, air, light, and other food components. Researchers' curiosity has grown as they try to figure out the best way to increase the absorption of astaxanthin in the body. As a result, scientists are creating novel encapsulating technologies to address these problems and to raise astaxanthin's water solubility, stability, activity, and bioavailability [5].

There is a variety of approaches that can be employed in pharmaceutical applications for diagnostic and therapeutic purposes, including microencapsulation [7], inclusion into liposomes [8], encapsulation into nanostructured liquid carriers (NLCs) [9], solid lipid nanocarriers (SLNs) [10], carbon nanotubes [11], micelles, polymer nanoparticles, and nano emulsion [12]. A chitosan matrix crosslinked with glutaraldehyde was used by Higuera-Ciapara and his colleagues to microencapsulate astaxanthin with increased stability [13]. The use of chemical crosslinking agents, however, was not safe for daily consumption and the microsized particles did not distribute well in water or increase the efficiency of cellular uptake [14]. Anarjan et al. produced astaxanthin colloidal particles with better cellular absorption than pure astaxanthin to obtain water dispersible astaxanthin [15]. Among them, adding astaxanthin to cubosomes using certain polymers is a promising method for combating the compound's limited bioavailability. According to studies, cubosomes have led to the improved drug delivery of entrapped drugs at the targeted site and have regulated the drug release, with lessened drug-related side effects [16]

Cubosomes have recently received extensive attention due to the growing interest in the field of pharmaceutical nanotechnology as a potential alternative drug carrier for the targeted delivery of pharmaceutical bioactives such as peptides, antibiotics, antimuscarinic drugs, enzymes, and analgesic delivery. They were more common than other nanocarriers such as liposomes due to their unique qualities, which included stabilizing the loaded molecule, having a larger drug loading capacity, and having a wider range of applications. Cubosomes are unique submicron bicontinuous nanostructured liquid crystalline particles with sizes ranging from 100 to 300 nm. Visually, these are solid, optically isotropic, and thermodynamically stable nanocarriers. In the structure of cubosomes, the bicontinuous lipid bilayers are arranged three dimensionally in a honeycomb shape and two interior aqueous channels provide room for different bioactive components. They have abilities to encapsulate various active molecules of hydrophilic, hydrophobic, and amphiphilic natures, enhancing bioavailability and minimizing side effects.

The ability of cubosomes as nanoparticles to bind hydrophilic, hydrophobic, and amphiphilic pharmaceutical substances is their main advantage. According to the literature, cubosomes have a number of other advantages that make them ideal for use in the development of novel drug carriers. Bioavailability, biocompatibility, bioadhesion, drug molecule defense against hydrolysis, oxidation, protein molecule defense against precipitation, denaturation, surface adsorption, and aggregation are the major outcomes of these lipid-based drug delivery systems. They have moreover demonstrated over a lengthy period of time that they are a reliable delivery mechanism. Patient adherence and their response to these therapies are the major challenges, for them the cubosomes are oriented correctly [17]. Additionally, this product has a long shelf life due to its bioadhesiveness, improved skin penetration, ease of formulation, higher drug carrying capacity, improved stability at any level of dilution, higher stability against breakage, and protection of dangerous pharmaceuticals. It is cost-effective, reliable, biocompatible, and risk-free [18].

Colloidal monoglyceride dispersions can be created utilizing a number of efficient methods, such as emulsification, precipitation, and high-energy fragmentation, although there is a knowledge gap about the cubosome preparation in terms of the formulation

elements and process parameters to maximize transition into the cubic phase, with reduced aggregation and improved drug entrapment [19].

Poloxamer 407 was chosen as a polymer for this study because of its biodegradable, biocompatible, and nontoxic properties [20]. However, without the support of research on physicochemical features, the construction of an optimal formulation is insufficient. It is important to carry out a physicochemical characterization of cubosomes to learn how our body responds to these small sized particles, especially because the cubosomes' fate in the body is largely determined by the surface area and particle size of the nanoparticles. Cubosomes' absorption, distribution, retention, and elimination are all influenced by the particles' surface and size, which are crucial in the synthesis. In addition, the structural state of cubosomes significantly affects their solubility and bioavailability to an extent and, to a lesser extent, their bioavailability [20]. In the industry, cubosome characterization is helpful for scaling up. Earlier studies have looked into a variety of cubosomal preparation development techniques; but, to the best of our knowledge, fabrication techniques have received the most attention. As a result, the purpose of the study is to assess the physicochemical characterization of recently developed lipid-based cubosomal formulations that are suggested for oral administration. An evaluation of the entrapment effectiveness, morphology, thermal characteristics, zeta potential, particle size, Fourier transform infrared (FTIR) spectroscopy, and X-ray diffraction (XRD) was carried out [21]. The results of this experimental study will give valuable insight into the physicochemical characterization of astaxanthin-loaded cubosomes developed using a different method to enhance astaxanthin bioavailability.

2. Materials and Methods

Glyceryl monooleate (GMO) was provided by the Mohini organics Pvt. Ltd. Mumbai as a gift. The polymer poloxamer 407 (Sigma-Aldrich Pvt. Ltd., St. Louis, MO, USA) was provided by the university. The astaxanthin extract (1.4% w/v) was purchased from the SVAgro food, Navi Mumbai, India. The DPPH was purchased form Sigma-Aldrich Pvt. Ltd., St. Louis, MO, USA. However, the remaining solvents, such as DMSO and methanol, were purchased from Loba Chemicals, Maharashtra, India. All the chemicals used were laboratory reagent grade.

3. Preparation Method of Cubosomes

Astaxanthin-loaded cubosomes (AST-LC) were prepared via a top-down approach (fabrication method). Accurately, weight quantities of GMO and poloxamer 407 were mixed in different ratios and melted at 60 °C in a hot water bath until the poloxamer 407 completely dissolved in the GMO. To the above solution, astaxanthin extract was added and mixed well. After that, 10 mL of preheated distilled water was added dropwise gradually to obtain a clear lipid solution by uninterrupted stirring (Figure 1). To ensure homogeneity, the mixture was vortex mixed at room temperature and equilibrated for 48 h. The dispersion appeared as a uniform opaque-colored mixture without any visible sign of aggregation. After 48 h, the entire mixture was subjected to homogenization at 1200 rpm for 2 h at room temperature. The mixture was distributed by mechanical stirring by adding 15 mL of distilled water. The final dispersion was examined under microscope and further lyophilized using lyophilizer stored in a glass vial at room temperature protected from direct sunlight [22].

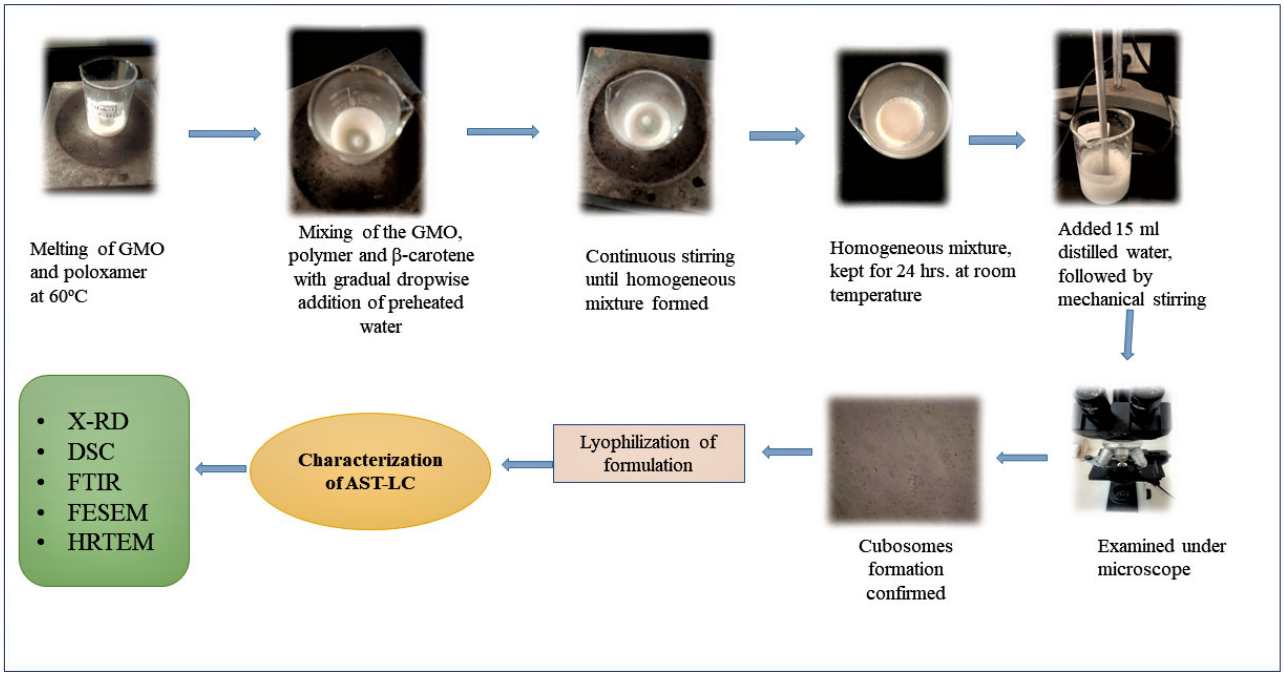

Figure 1. Illustration of fabrication method (top-down approach).

4. Physicochemical Study of Astaxanthin-Loaded Cubosomes (AST-LC)

4.1. Physicochemical Characterization of Astaxanthin-Loaded Cubosomes

Physicochemical characterization of astaxanthin-loaded cubosomes was performed through encapsulation efficiency (EE), measurement of particle size and their distribution, and zeta potential. The morphology of the astaxanthin-loaded cubosomes was visualized via X-ray diffraction (XRD), high resolution transmission electron microscopy (HRTEM), field emission scanning electron microscopy (FESEM), and diffraction scanning calorimetry (DSC) [23].

4.1.1. Visual Examination

Prepared formulations were visually examined for color, turbidity, homogeneity, and presence of microscopic particles. Well-dispersed samples contained no visible signs of aggregates and contained homogeneous consistency.

4.1.2. Percentage Yield and Entrapment Efficiency

The prepared cubosomes were collected and weighed accurately. The percentage yield was determined by dividing the formulation weight by the total weight of the excipients and extracts [24]. The formula for calculating percentage yield is given in Equation (1).

For the determination of entrapment efficiency, an accurate amount of astaxanthin-loaded cubosomes was dissolved in the PBS pH 7.4 and then kept in an orbital shaker at 100 rpm at 37 °C temperature for 24 h. After mixing the solution, it was centrifuged for 20 min at 4000 rpm. The supernatant was collected and spectrophotometrically measured at 460 nm. Then, working dilutions were made for calibration curve and scanned at the same λ_{max} to determine the drug concentration in the formulation [25]. The entrapment efficiency was calculated using the formula given in Equation (2).

$$\% \text{ yield} : \frac{\text{total weight of cubosomes}}{\text{total weight of excipients} + \text{drug}} \times 100 \quad (1)$$

$$\text{Entrapment efficiency} : \frac{\text{total drug added} - \text{free drug}}{\text{total drug added}} \times 100 \quad (2)$$

4.1.3. Determination of Particle Size, Zeta Potential, and Polydispersity Index (PDI)

The zeta sizer nano-series (Zetasizer 2000 HS, M/s Malvern Instruments Limited, Malvern, UK) was used to evaluate the particle size, zeta potential, and PDI of the produced cubosomes [26]. Deionized water was used to dilute the sample in the cuvette, before measurements were taken at 25 °C. When particles move with a Brownian motion, their diffusion is measured by DLS and converted to size and distribution using the Stokes–Einstein relationship. The surface charge of the cubosomal dispersion was measured using the zeta potential method, which also predicts the cubosomes' in vivo stability. Higher repulsion is produced by the zeta potent ion, showing better stability of the developed dispersion. The bigger size distribution in the particle sample corresponds to PDI, which was determined by the cumulative analysis of the zeta sizer values. After dispersing nanoparticles in distilled water at 25 °C, the zeta potential and particle size were measured in triplicate [27]. The reported value for the mean diameter of the average particle size (n = 3) was stated as SD.

4.1.4. Optical Microscopic View of the Cubosomes

Using an electron microscope with a 45× magnification, the produced vesicles were examined for surface morphology. A drop of the dispersion was applied to the glass slide and any excess was drained off using filter paper and let to dry. Then, an optical microscope was used to study the sample to see how the vesicles had formed [28].

4.1.5. Field Emission Electron Microscopy (FESEM)

FESEM was utilized to examine the surface morphology in more detail (S-3400 N, Hitachi, Japan). A drop of the sample was applied to the glass coverslip that was taped to an aluminum stub for the SEM investigation. After about 30 min of air drying, the drop was viewed with a scanning electron microscope [29].

4.1.6. High Resolution Transmission Electron Microscope (HRTEM)

Using a JEM 2100 PLUS JEOL instrument, TEM (transmission electron microscopy) pictures were taken. Samples were made by dropping 10 L of cubosomes onto a copper grid with 10% phosphotungstic acid. The size distribution was figured out by using software to look at an overall TEM image [30].

4.1.7. Diffraction Scanning Calorimetry (DSC)

DSC is one of the calorimetric methods most often used to describe how soluble the drug is and what its physical state is. A differential scanning calorimeter was used to record the thermograms of astaxanthin extract, poloxamer 407, GMO, a physical mixture of all the ingredients, and astaxanthin extract-loaded cubosomes (AST-LC). The samples (5 mg) were heated throughout, from the 30–500 °C range of temperature at a rate of 10° k/min, using alumina as a reference standard under a nitrogen environment after being sealed hermetically in aluminum pans having flat surfaces [31].

4.1.8. Powder X-ray Diffraction

X-ray diffraction is a technique used to characterize the internal structure of the drug substance. This procedure helps to find out changes in the internal structure of the drug substances that may takes place due to an altered environment. An X-ray diffractometer was used to obtain the XRD patterns of astaxanthin extract, polymer, and astaxanthin-loaded cubosomal formulation. Diffractograms were recorded using Cu as the tube anode under the following conditions: current 30 mA, voltage 45 kV, at 0.02° (°2Th), at a counting rate of 0.5 s/step at room temperature, and data collection was carried out from 4 °C to 40 °C [32].

4.1.9. Fourier Transformed Infrared (FTIR) Spectroscopy

The infrared spectrum of drugs or any compound provides the information about functional groups present in the compound. The FTIR of the carotenoid extracts, GMO, poloxamer 407, physical mixture of all, and AST-LC were recorded using an IR spectrophotometer. A total of 2 mg/200 mg KBr of the samples were prepared in a KBr disc with hydrostatic press. The prepared pellets were scanned in the range of 4000–400 cm^{-1} [28].

5. In Vitro Release and Evaluation of the Release Mechanism

The dialysis method was used to assess the release of AST-LC in a phosphate buffer of pH 7.4 at 37 °C. The 900 mL of phosphate buffer with a pH of 7.4 was added to a flask, along with the 5 mL of cubosomal sample that contained 50 mg of the drug. The flask was then placed in an incubator shaker, rotating at 50 rpm and 37 °C. Periodically, a 5 mL sample was removed and replaced with a phosphate buffer solution in the same volume. The amount of drug release at specific time intervals was calculated using the absorbance obtained when samples were taken out and evaluated by a UV spectrophotometer at 483 nm. In addition, the in vitro drug release was assessed at pH 1.2 for 2 h and at pH 6.8 for 36 h, following the same procedure. Additionally, the formed cubosomes' drug release kinetics and mechanism were calculated using the Excel add-in DDSolver. To ascertain the drug release behavior from the developed formulations, a variety of release models, including zero-order, first-order, Higuchi, Hixson Crowell, and Korsmeyer–Peppas models, were used [33]. The following mathematical equations of various release models were used:

Zero-order model: $Q = K_0t + Q_0$
First order model: $Q = Q_0e^{k1^t}$
Higuchi model: $Q = k_Ht^{1/2}$
Korsmeyer–Peppas model: $Q = k_{KP}t^n$

The rate constants for the release of astaxanthin in the zero-order, first-order, Higuchi, and Korsmeyer–Peppas models, respectively, are k_0, k_1, k_H, and k_{KP}. Q and Q_0 denote the amount of astaxanthin released at time points t and 0, respectively. In addition to this, n represents the release exponent, which suggests the process of astaxanthin release. If the value of n= 0.5, that means the drug release follows Fickian diffusion, the value of n between 0.5 and 1.0, the diffusion mechanism is non-Fickian or anomalous, the value of n = 1.0, then Non-Fickian case II diffusion has been followed and for n > 1.0 a non-Fickian super-case II diffusion process has been followed. In order to find the formulations that best fit the release profile, the Akaike index criteria (AIC) were established. The quality of fit was chosen based on the information from the AIC and the regression coefficient [34].

6. Anti-Oxidant Activity

DPPH Radical Scavenging Activity

The scavenging activity against free radicals is being tested in this assay. The decrease in the stable free radical DPPH's absorbance at 517 nm can be used to assess the scavenging capacity of natural compounds. The reaction between the purple free radical and the scavenger results in the colorless compound 1,1-diphenyl-2-picrylhydrazine [35].

For the DPPH assay, 3 mL of astaxanthin-loaded cubosomes (AST-LC) with concentrations ranging from 20, 40, 80,100, 200, 400, and 800 µg were mixed with 1 mL of 0.1 mM DPPH methanolic solution. The astaxanthin extract in DMSO was adjusted to the same concentration as the AST-LC. Then, the solution was incubated at 37 °C in the dark for 40 min. An amount of 1 mL of DPPH in 3 mL of methanol was used as the control and methanol and DMSO were used as the sample blank for AST-LC and astaxanthin extract, respectively. Using a UV spectrophotometer, the absorbance of the sample and the control was determined at 517 nm [36]. The sample mixture's low absorbance suggested that it had

a strong capacity to scavenge free radicals. The following formula was used to estimate the proportion of DPPH-scavenging activity:

$$DPPH\ sacvenging\ (\%) = \frac{A_{control} - A_{sample}}{A_{control}} \times 100$$

7. Result and Discussion

7.1. Percentage Practical Yield and Entrapment Efficiency

A yield of 87.5% was achieved. Following the separation of the free drug from the cubosomal nano-formulations loaded with the drug, the EE (%) of the astaxanthin-loaded cubosomes was calculated. The obtained EE (%) was 87.6 ± 2.13%, indicating that the majority of the extract was entrapped within the cubosomes. It was speculated that this would happen because astaxanthin is hydrophobic and soluble in GMO and therefore would be trapped in the cubosomes' hydrophobic channels. All the measurements were carried out in triplicate.

7.2. Particle Size and Polydispersity Index

In general, poloxamer 407 added to the cubosomal dispersion medium resulted in negative charge values of cubosomes due to the interaction between the poloxamer 407 hydroxyl ions and the aqueous medium. The resulted particle size might be due to the presence of the GMO and poloxamer 407. The astaxanthin-loaded cubosomes (AST-LC) had a minimal polydispersity index (0.283 ± 1.01) and an average particle size of 199 ± 0.23 nm, indicating a uniform micelle size. From the previous studies, it is clear that the particle size is mostly affected by the ratio of the drug to the dispersed phase; the particle size increases as the ratio increases. Moreover, this particle size indicated that, during homogenization, the bulk gels were disrupted, resulting in this size of particles. The low concentration of poloxamer 407 was responsible for the obtained particle size. It was stated in various studies that higher zeta potential levels provide enough electric repulsion that prevents particle aggregation. The observations of the zeta potential demonstrate that astaxanthin-loaded cubosomes (AST-LC) contained a negative charge, with mean values ranging from −27.9 to −29.1. (Figures 2 and 3). It was hypothesized that the hydroxy ion of poloxamer 407 interacted with the aqueous medium, causing cubosomes to generally have negative charge values after being added to the cubosomal dispersion medium.

7.3. Microscopic View of the Cubosomes

The prepared formulation has been examined under optical microscope to confirm vesicle formation, as shown in Figure 4.

7.4. FESEM of Astaxanthin-Loaded Cubosome (AST-LC)

The size and surface appearance of the astaxanthin-loaded cubosomes (AST-LC) were examined using the FESEM. On a copper grid, the cubosomal dispersion was positioned in the appropriate slot. The SEM (Hitachi, Tokyo, Japan: Model: SU8010 SERIES) was used to take the photomicrographs for determining the size and surface of cubosomes. According to the photomicrographs obtained, the AST-LC were identified as having a smoother surface and a cubical shape (Figure 4).

7.5. High Resolution Transmission Electron Microscopy (HRTEM)

The cubic nanostructures in the formulation sample were visible due to the high TEM magnification power [37]. The cubic nanoparticles with the typical cubosome structure are shown in Figure 4. TEM images of astaxanthin-loaded cubosomes (AST-LC) showed the irregular distribution of hexagonal- to cubic-shaped discrete particles. The particles are isolated from each other, ensuring their stability.

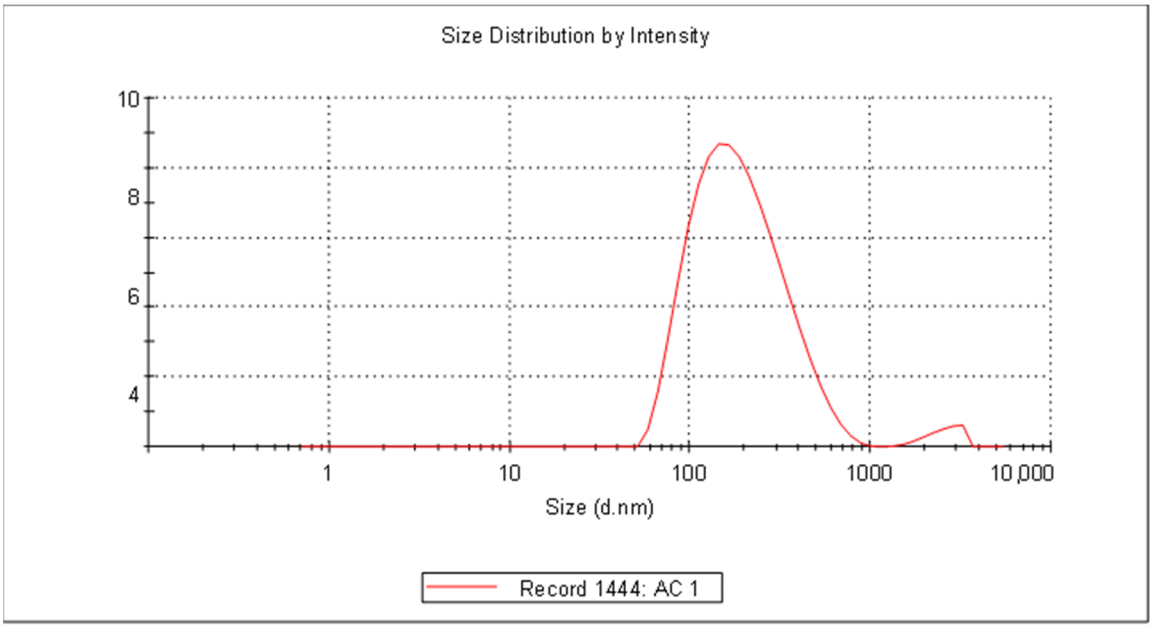

(**a**)

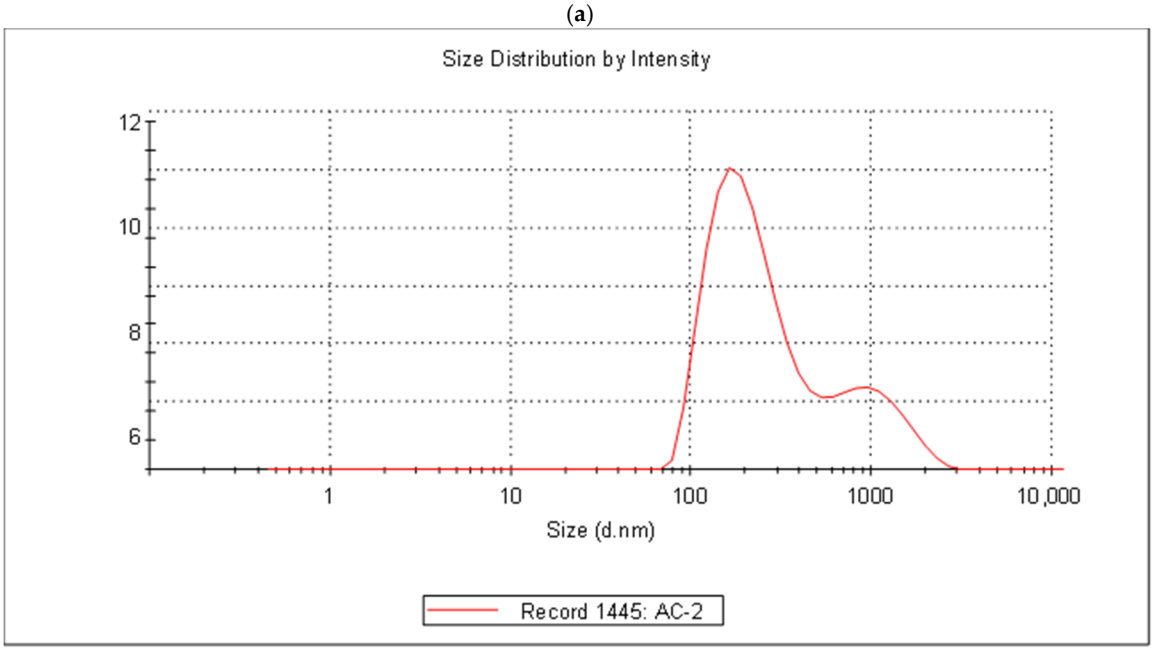

(**b**)

Figure 2. *Cont*.

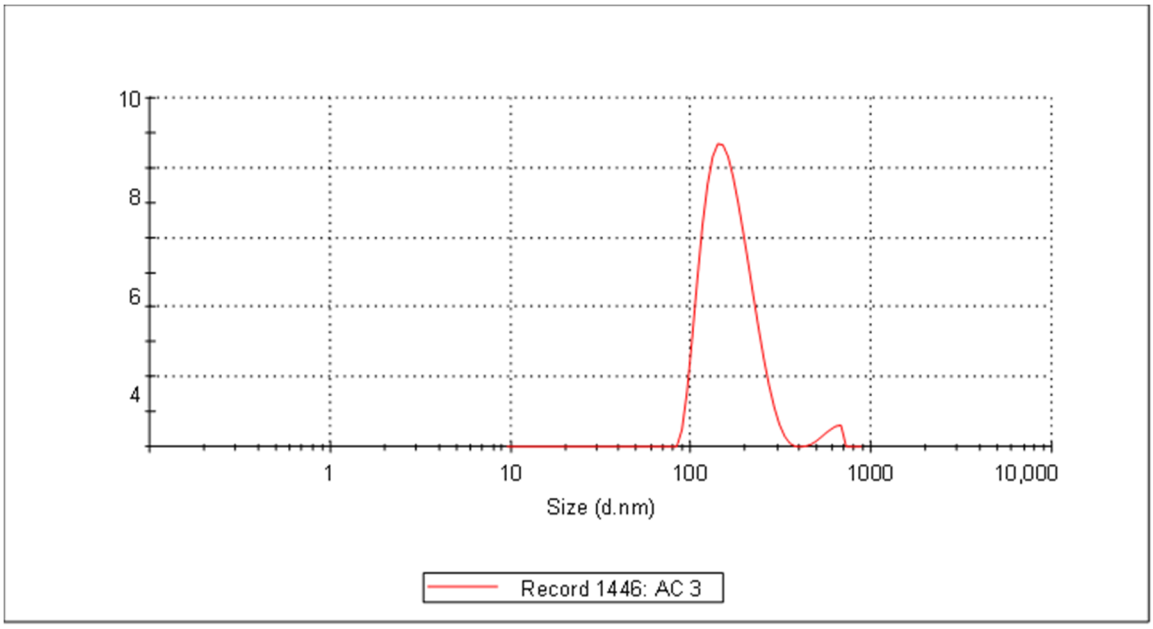

(**c**)

Figure 2. Particle size of AST-LC (**a**) Z-Average (d.nm): 199.2 and PdI: 0.29; (**b**) Z-Average (d.nm): 198.0 and PdI: 0.287; (**c**) Z-Average (d.nm): 189.5 and PdI: 0.27. The vertical axis denotes intensity in %. PdI—polydispersity index.

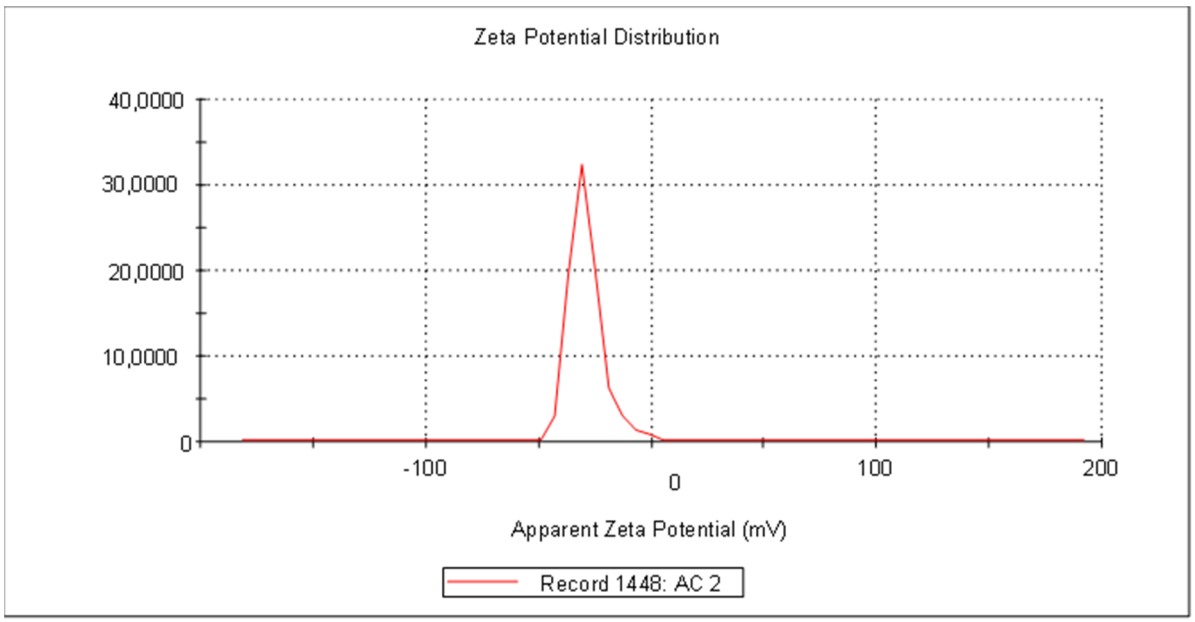

(**a**)

Figure 3. *Cont.*

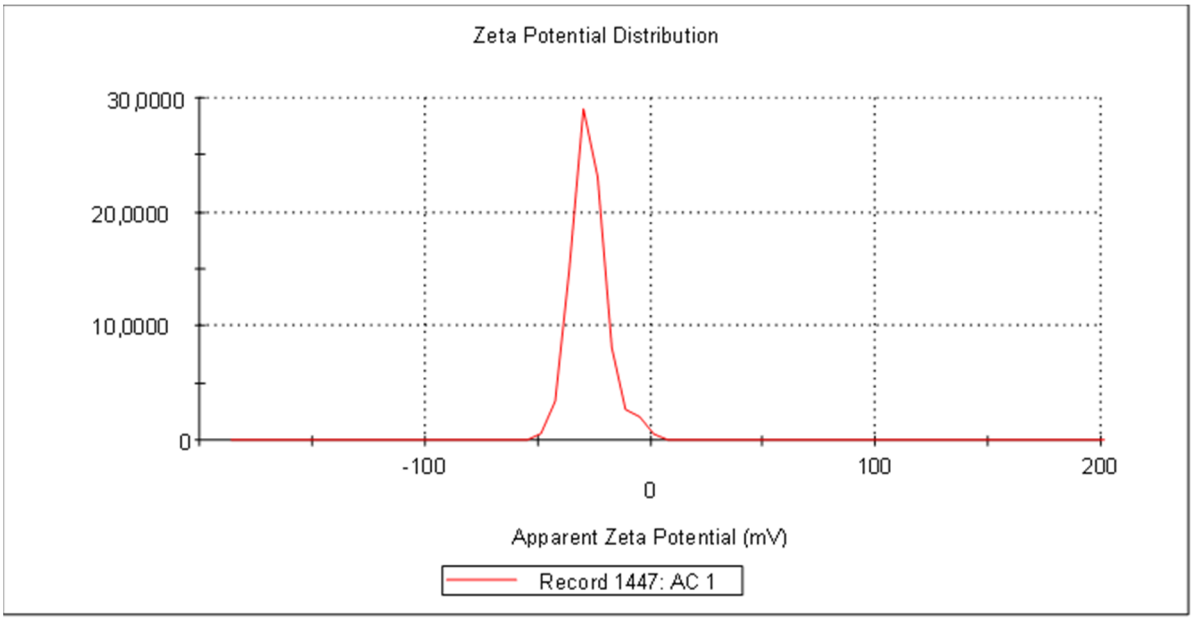

(**b**)

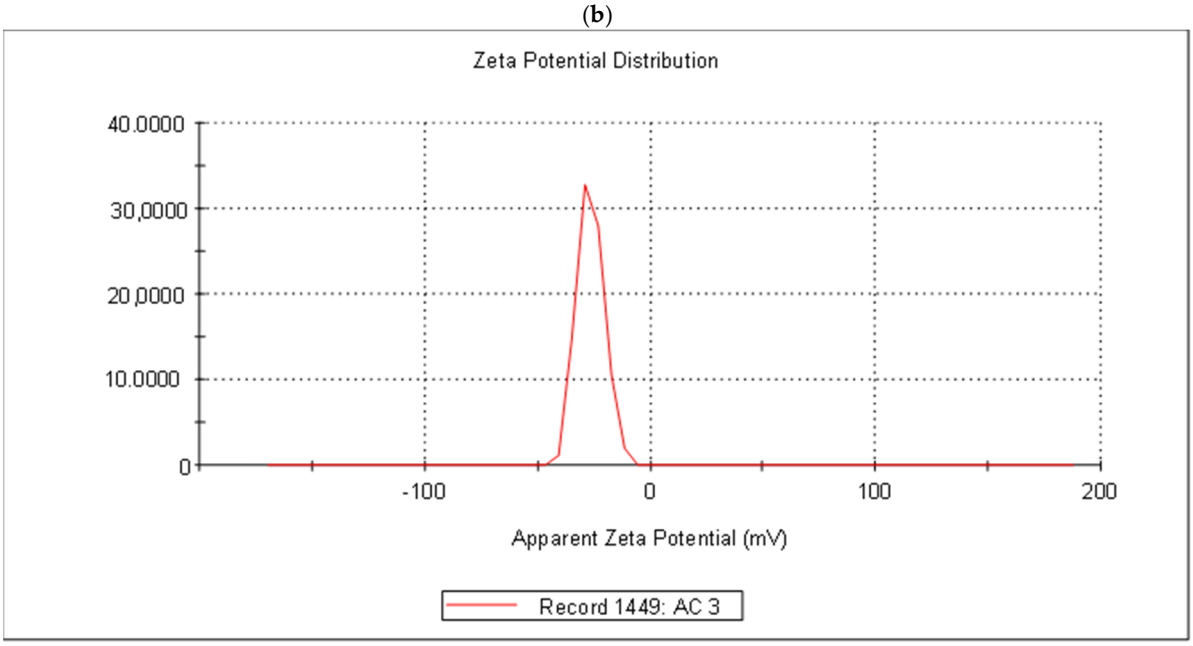

(**c**)

Figure 3. Zeta-potential of AST-LC: (**a**) −29.1; (**b**) −28.9; (**c**) −27.9. The vertical axis denotes total counts per seconds.

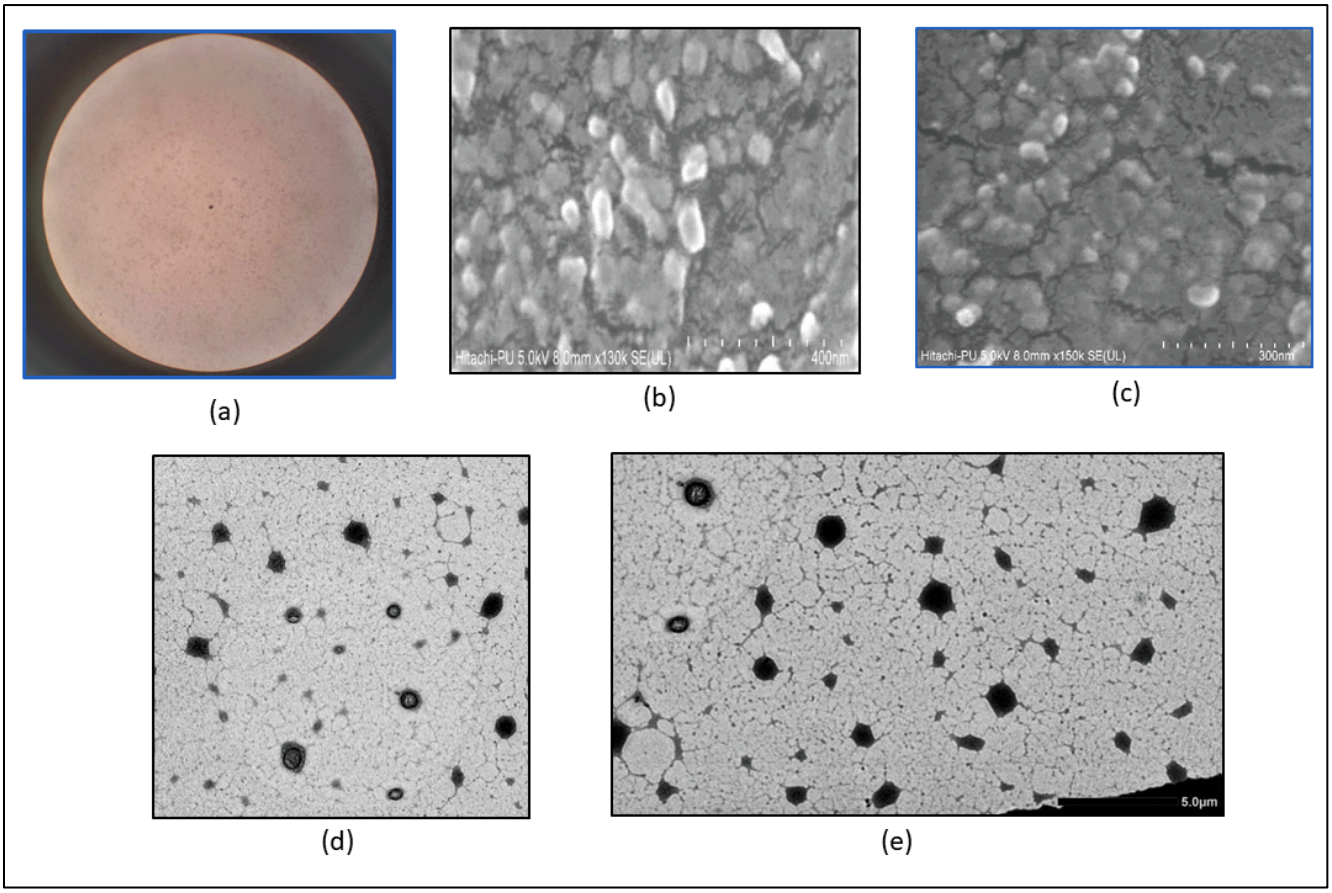

Figure 4. Morphology of AST-LC. (**a**) Optical microscopic view of AST-LC, (**b**,**c**) FESEM images of AST-LC, (**d**,**e**) HRTEM images of AST-LC.

7.6. Diffraction Scanning Calorimetry Thermogram

Figure 5 shows the DSC thermograms of astaxanthin (Figure 5a), GMO (Figure 5b), poloxamer407 (Figure 5c), physical mixture of drug and excipients (Figure 5d), and astaxanthin-loaded cubosomes (Figure 5e). The DSC thermogram of the astaxanthin exhibited a distinct characteristic endothermic peak at 220 °C, corresponding to its melting point, reflecting the crystalline state of the drug. The DSC thermogram of the GMO showed an endothermic peak at 37 °C, while that of poloxamer 407 showed an endothermic peak at 57 °C. The physical mixture of astaxanthin, GMO, and poloxamer 407 exhibited all the peaks of the excipients as well as the drug, indicating no signs of interaction. The AST-LC did not show a drug peak. However, a peak corresponding with the polymer peak is present, confirming the complete incorporation of astaxanthin into the nanostructures. These results revealed that the astaxanthin, when incorporated into the cubosomal nanoparticles, may be in the amorphous form or it may be molecularly dispersed inside the cubic nanostructure.

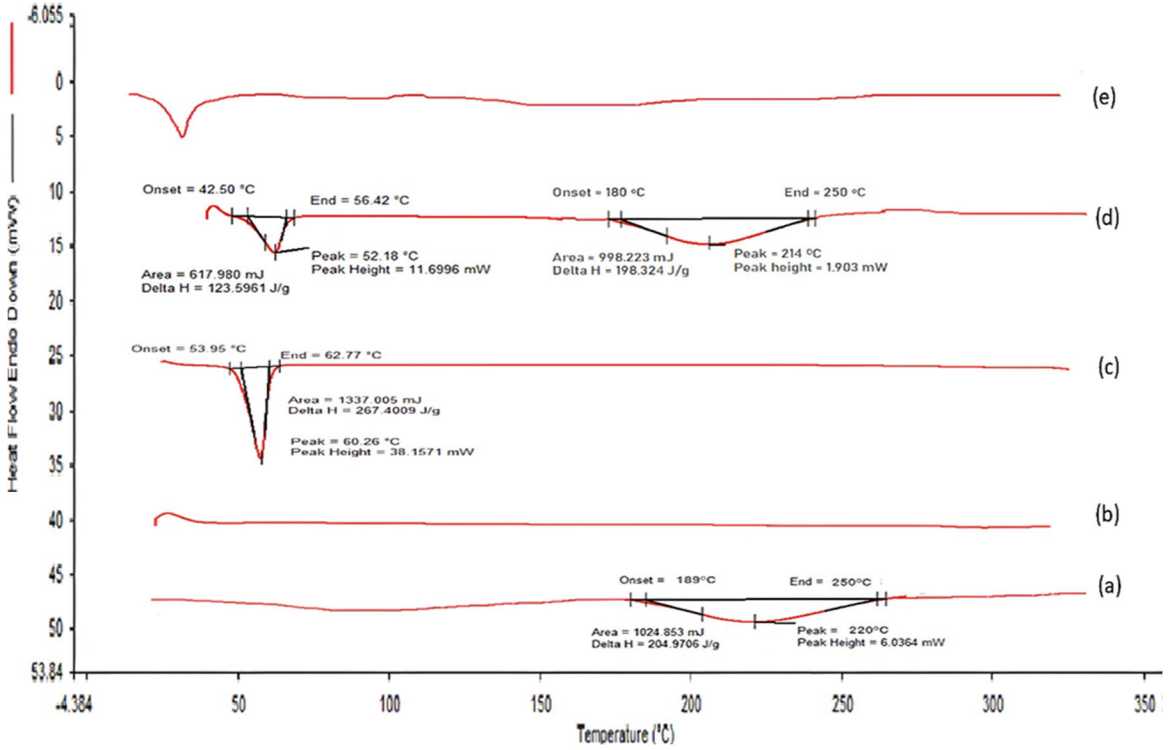

Figure 5. Diffraction-scanning calorimetry (DSC). (**a**) Astaxanthin extract; (**b**) glyceryl monooleate (GMO); (**c**) poloxamer 407; (**d**) physical mixture of astaxanthin, GMO, and poloxamer 407; (**e**) astaxanthin-loaded cubosomes.

7.7. Powder X-ray Diffraction

To verify the physical state of astaxanthin (Figure 6a), poloxamer 407 (Figure 6b), and astaxanthin incorporated into cubosomes (Figure 6c), X-ray diffraction was used. Poloxamer 407 displayed two distinct peaks at 19.3 and 23.3 nm, demonstrating the crystal structure of the compound. In addition, the crystalline structure of astaxanthin was revealed from the diffractogram of astaxanthin extract, which showed many distinctive intensity reflection peaks between 10 and 50° (2 = 16.3, 18.2, 20.5, 22.7, 23.5, 25.5, 31.9, and 32.2°), although in the astaxanthin-loaded cubosomes' X-ray diffraction pattern these distinctive peaks vanished (AST-LC), reflecting the incorporation of the drug into the cubosomes. This supports earlier DSC study findings and suggests that the astaxanthin was molecularly distributed, or in its amorphous form, when encapsulated into the cubosomes.

7.8. Fourier Transformed Infrared (FTIR) Spectroscopy

The FTIR of the astaxanthin extract (Figure 7a), GMO (Figure 7b), poloxamer 407 (Figure 7c), physical mixture (Figure 7d), and AST-LC (Figure 7e) was given. The astaxanthin extract displayed –OH stretch at 3157.36 cm^{-1}, –C–H stretch at 2933.56 cm^{-1}, –C=O stretch at 1592.29 cm^{-1}, and R_2–C=C–R at 597.30 cm^{-1}. The characteristic peak, i.e., the C–H stretch aliphatic peak of poloxamer 407, was obtained at 2887 cm^{-1}. Other peaks, such as O–H bend and C–O stretch were found at 1343.42 cm^{-1} and 1110.62 cm^{-1}, respectively. Additionally, GMO showed absorption peaks at 1739.78 cm^{-1} for C=O stretch, 2853 cm^{-1} for C–H stretch, 3380.75 cm^{-1} for O–H stretch, 1460 cm^{-1} for O–H bending, and 2922.68 cm^{-1} for C–H stretch of alkene. The FTIR of the physical mixture did not show any extra peaks, except the drug and excipients, revealing an absence of any interaction between them. Likewise, the spectra of drug-loaded cubosomes showed a complete disappearance of the characteristic peak of astaxanthin, revealing its incorporation into the cubosomes, supporting the results of DSC and XRD.

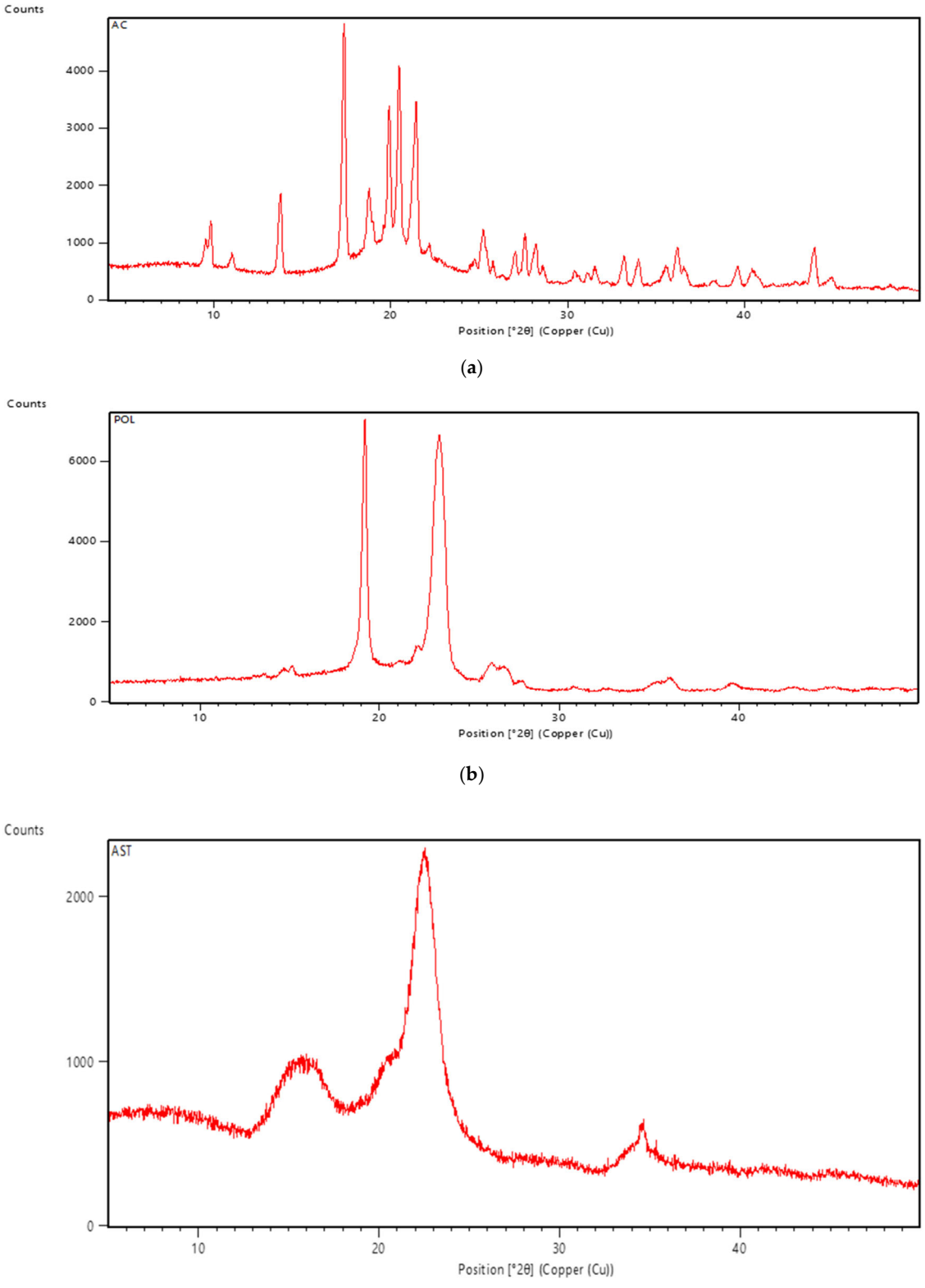

Figure 6. XRD spectra of (**a**) astaxanthin extract, (**b**) poloxamer 407, and (**c**) astaxanthin-loaded cubosomes (AST-LC).

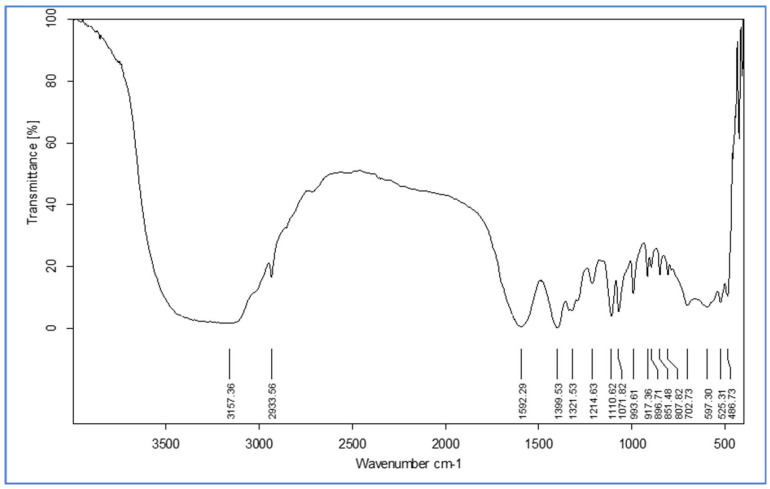

(**a**)

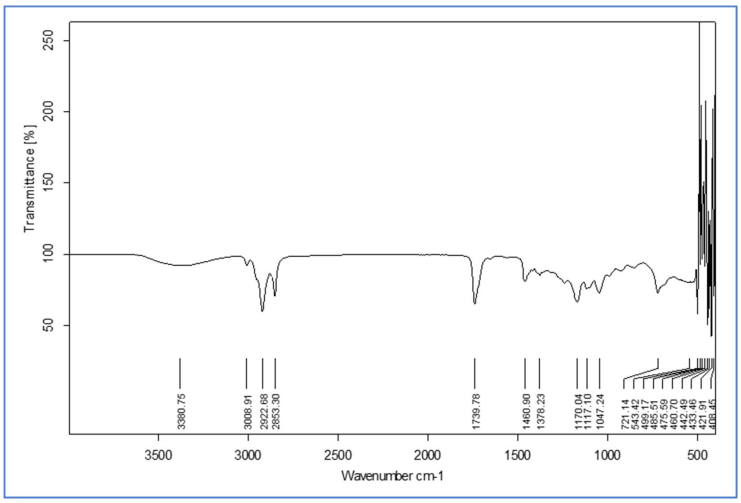

(**b**)

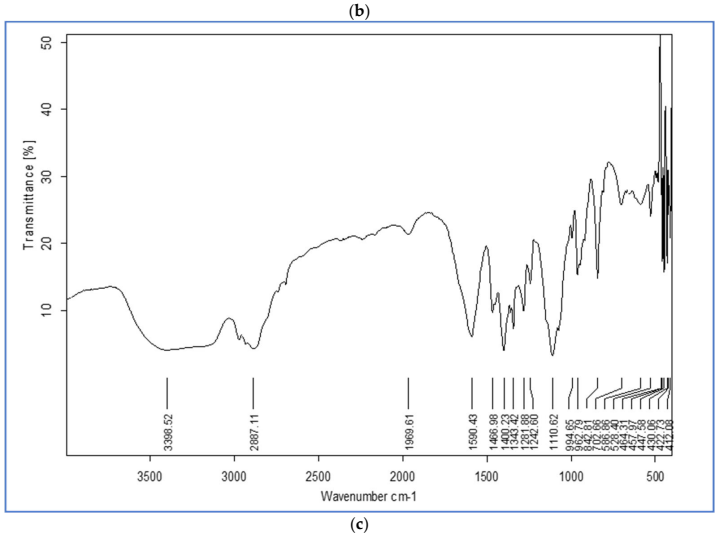

(**c**)

Figure 7. *Cont.*

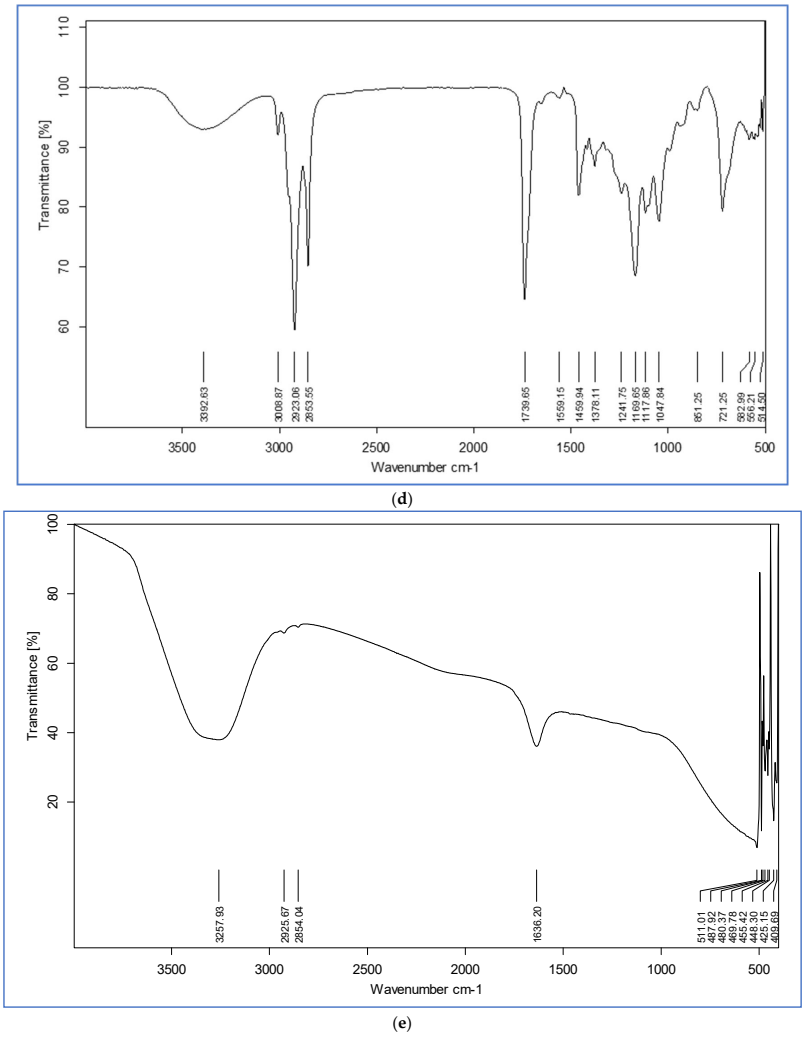

Figure 7. Fourier transformed infrared (FTIR) spectroscopy of. (**a**) Astaxanthin extract; (**b**) GMO; (**c**) poloxamer 407; (**d**) physical mixture of astaxanthin extract, GMO, and poloxamer 407; (**e**) astaxanthin-loaded cubosomes (AST-LC).

7.9. In Vitro Release Study

The release kinetics of the encapsulated drugs in a nanoparticle are a crucial factor for evaluating the successful development of the nanoparticle formulations. At pH 1.2, a 12.32% drug release in 2 h was obtained, while at pH 6.8, a 35.24% drug release was noted within 6 h, and a 97.34 ± 4.32% drug release within 36 h. The initial burst release from the cubosomes occurred within the first 2 h, followed by a steady release pattern for the following 36 h. This biphasic release pattern had clinical significance, since the first assertive drug release resulted in a quick commencement of action, whereas the extended gradual drug release caused the drug delivery over a long time period. The persistent drug release behavior may be attributable to drug diffusion through the water channels within the cubic structures, whereas the initial drug release might be due to the absorption of the drug on the cubic surface, resulting in an immediate release of the drug to the matrix. The tortuosity and the narrow pore size of the inner aqueous nanochannels of the cubic nanoparticles were responsible and contributed to the slowing down of the release of the drug.

When astaxanthin-loaded cubosome (AST-LC) dispersions were subjected to in vitro drug release conditions, they demonstrated a sustained release profile with a cumulative drug release ranging around 99.7 ± 1.43% over 36 h of study (Figure 8a). The linear regression analysis with zero-order, first-order, Higuchi, Hixson-Crowell, and Korsmeyer–Peppas

models were used to check the release kinetics of the designed cubosomes' preparation (Figure 8, Table 1). The results shown in the table were determined to best fit the Higuchi model (R^2 = 0.94) and the Korsmeyer–Peppas model with the linear regression r^2 value; the release exponent (n) was found to be 0.77 (n = 0.5 < n < 1.0), indicating that the drug release followed a non-Fickian or anomalous diffusion process. Cubosomes, which are discrete, submicron-, or nanostructured particles created by fragmenting cubic phase gels, have a large specific surface area that increases the likelihood that astaxanthin will diffuse from the lipid bilayers and cause a sustained release. The particle size and the three-dimensional cubic structure of the cubosomes, which provide a huge surface area, are some factors responsible for the sustained and complete drug release over time.

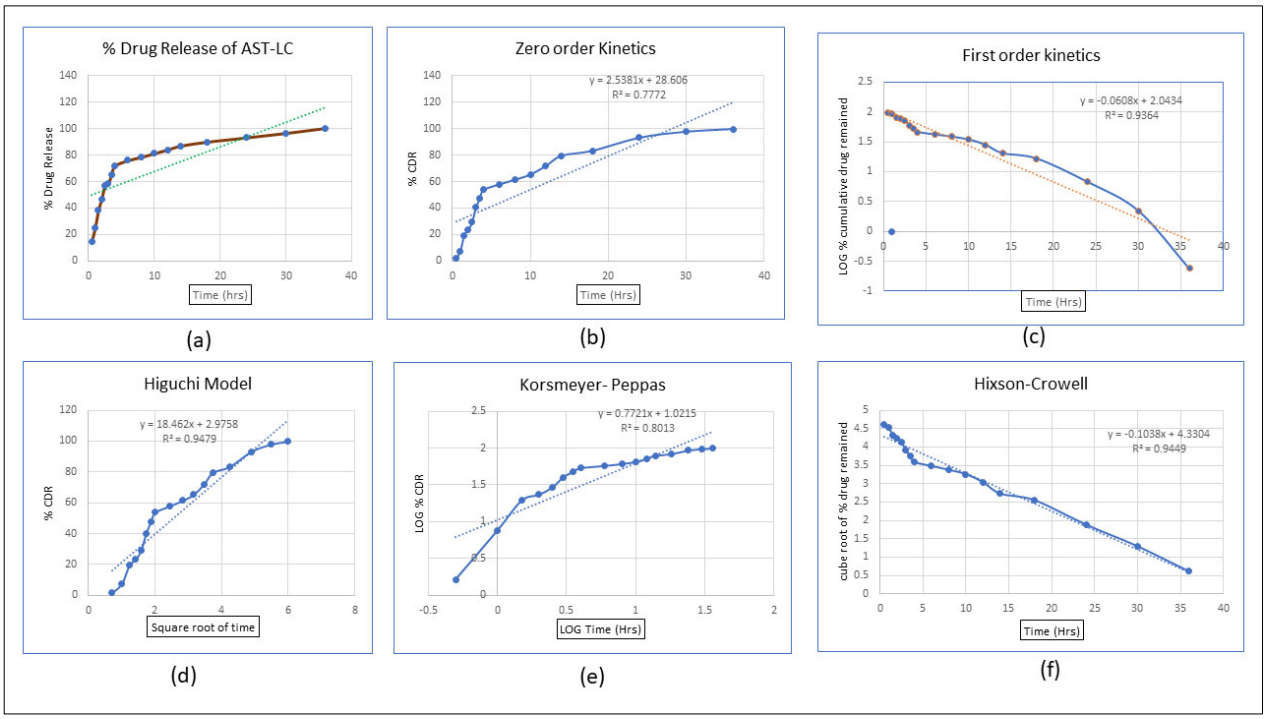

Figure 8. Showing % CDR and graphs of pharmacokinetic parameters. (**a**) % CDR of drug from AST-LC with respect to time; (**b**) zero-order kinetics; (**c**) first-order kinetics (**d**) Higuchi kinetics; (**e**) Korsmeyer–Peppas model; (**f**) Hixson–Crowell model.

Table 1. In vitro release parameters of different release models.

Formulation	Zero-Order		First-Order		Higuchi		Korsmeyer–Peppas			Hixon–Crowell	
AST-LC	r^2	k_0	r^2	k_1	r^2	k_H	r^2	n	k_{KP}	r^2	k_{HC}
	0.777	2.538	0.9364	−0.060	0.9479	18.462	0.8013	0.77	1.0215	0.9449	−0.103

7.10. DPPH Radical Scavenging Activity

The antioxidant activity was measured using the DPPH radical scavenging activity assay. After reacting with a free radical quencher, the DPPH radical changed from its deep violet color in the solution to a colorless or pale yellow. The basis of the DPPH assay method is the conversion of DPPH in an alcoholic solution to DPPHH in the presence of an antioxidant that donates hydrogen.

The DPPH activity of AST-LC was measured and, as expected, the scavenging activity was improved with an increase in concentration to some extent (100 µg/mL) because of the prooxidant effect exerted by the carotenoids. The prooxidant effect of the astaxanthin might be due to the increased concentration of the same when encapsulated in the cubosomes. The decrease of antioxidant activity of AST with the concentration increase might be due to

aggregation of the carotenoid. Astaxanthin is a xanthophyll carotenoid, well known for its ability to form J- or H-aggregates in the presence of water and even in lipid membranes. EPR-spin trapping experiments have shown that such aggregation results in the decrease in antioxidant activity of AST and other xanthophyll carotenoids. For astaxanthin extract, RSA% for 57.81 ± 5.42% was observed. However, when incorporated into cubosomes, the RSA% was significantly increased up to a concentration and found to be 76.18 ± 4.32%, as shown in Figure 9.

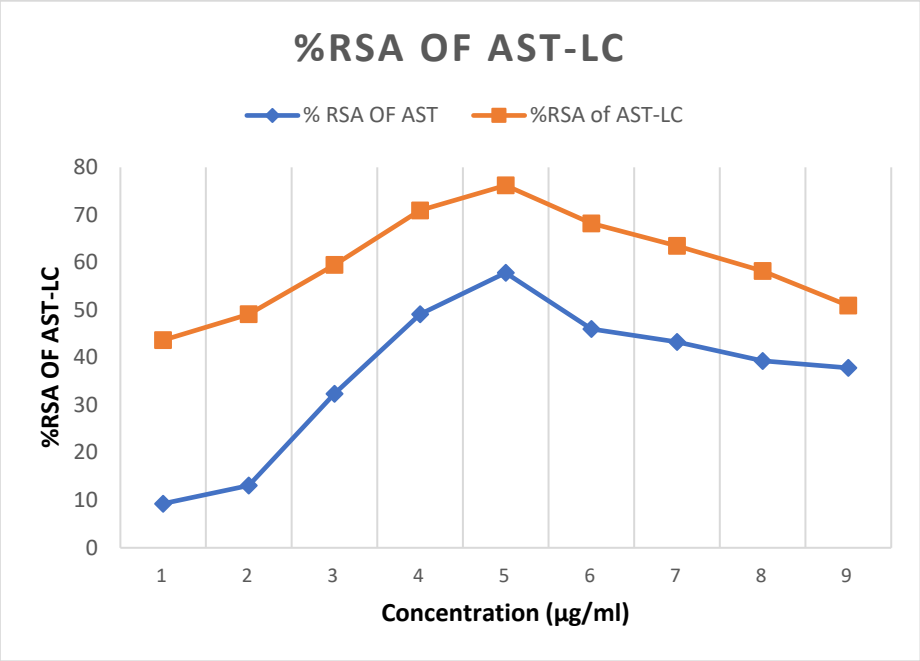

Figure 9. Showing RSA% of astaxanthin extract and BC-LC.

8. Conclusions

As an antioxidant, antiinflammatory, and antiapoptotic agent, astaxanthin has demonstrated a wide range of therapeutic actions. Although astaxanthin is effective in vitro and in vivo, its insolubility has prevented it from being used therapeutically. As a result, some recent research on various paradigms has shown an increased efficacy and bioavailability of astaxanthin. We were able to maneuver around this problem by integrating astaxanthin into a lipid-based nano-formulation and increasing its stability and solubility. This study concentrated on examining the physicochemical properties of astaxanthin-loaded cubosomes using various techniques. The results of the AST-LC formulation showed a particle size of 199 ± 0.23 nm, a modest polydispersity index of (0.283 ± 1.01), and −27.4 ± 4.67 mV zeta potential. By using FESEM and HRTEM, the cubic morphology of the formulation was further validated. In terms of yield and entrapment efficiency, the figures were 87.5% ± 1.08% and 87.6 ± 2.13%, respectively (n = 3). Furthermore, the astaxanthin becomes confined in an amorphous state, according to a DSC thermograph and an XRD spectrum of the cubosomes containing astaxanthin. Moreover, the absence of astaxanthin characteristic peaks in the FTIR results indeed confirmed the incorporation of the same within the cubosomes. In the DPPH assay, the AST-LC formulation (76.18 ± 4.32%) was found to possess significantly improved antioxidant potential compared with the pure astaxanthin extract (57.81 ± 5.42%). The findings of these investigations imply that the encapsulation of the astaxanthin extract into a lipid-based formulation may be able to improve astaxanthin bioavailability and antioxidant activities.

Author Contributions: Conceptualization, A.G. and R.K.S.; methodology, S.K.; software, S.K.; validation, A.G. and M.G.; formal analysis, S.K.; investigation, S.K.; resources, S.K.; data curation, S.K.; writing—original draft preparation, S.K.; writing—review and editing, S.K. and A.A.; visualization, A.G. and R.K.S.; supervision, M.G.; project administration, A.G.; funding acquisition, A.A. All authors have read and agreed to the published version of the manuscript.

Funding: The APC was funded by research funds of the University of Oradea.

Data Availability Statement: The data supporting the findings of this study are available within the article.

Acknowledgments: Authors are thankful to Chitkara University, Punjab, India for providing institutional facility.

Conflicts of Interest: The authors declare no conflict of interest.

References

1. Kumari, S.; Goyal, A.; Garg, M. Phytochemistry and Pharmacological Update on Tetraterpenoids. *Nat. Prod. J.* **2021**, *11*, 617–628. [CrossRef]
2. Li, X.; Matsumoto, T.; Takuwa, M.; Ali, M.S.E.S.; Hirabashi, T.; Kondo, H.; Fujino, H. Protective effects of astaxanthin supplementation against ultraviolet-induced photoaging in hairless mice. *Biomedicines* **2020**, *8*, 18. [CrossRef] [PubMed]
3. Chuyen, H.V.; Eun, J.-B. Marine carotenoids: Bioactivities and potential benefits to human health. *Crit. Rev. Food Sci. Nutr.* **2017**, *57*, 2600–2610. [CrossRef] [PubMed]
4. Mano, C.M.; Guaratini, T.; Cardozo, K.H.; Colepicolo, P.; Bechara, E.J.; Barros, M.P. Astaxanthin restrains nitrative-oxidative peroxidation in mitochondrial-mimetic liposomes: A pre-apoptosis model. *Mar. Drugs* **2018**, *16*, 126. [CrossRef]
5. Liu, C.; Liu, Z.; Sun, X.; Zhang, S.; Wang, S.; Feng, F.; Wang, D.; Xu, Y. Fabrication and characterization of β-lactoglobulin-based nanocomplexes composed of chitosan oligosaccharides as vehicles for delivery of astaxanthin. *J. Agric. Food Chem.* **2018**, *66*, 6717–6726. [CrossRef] [PubMed]
6. Gu, J.; Chen, Y.; Tong, L.; Wang, X.; Yu, D.; Wu, H. Astaxanthin-loaded polymer-lipid hybrid nanoparticles (ATX-LPN): Assessment of potential otoprotective effects. *J. Nanobiotech.* **2020**, *18*, 53.
7. Bustos-Garza, C.; Yáñez-Fernández, J.; Barragán-Huerta, B.E. Thermal and pH stability of spray-dried encapsulated astaxanthin oleoresin from Haematococcuspluvialis using several encapsulation wall materials. *Food Res. Int.* **2013**, *54*, 641–649. [CrossRef]
8. Kumari, S.; Goyal, A.; Sönmez Gürer, E.; AlgınYapar, E.; Garg, M.; Sood, M.; Sindhu, R.K. Bioactive Loaded Novel Nano-Formulations for Targeted Drug Delivery and Their Therapeutic Potential. *Pharmaceutics* **2022**, *14*, 1091. [CrossRef]
9. Tamjidi, F.; Shahedi, M.; Varshosaz, J.; Nasirpour, A. Design and characterization of astaxanthin-loaded nanostructured lipid carriers. *Innov. Food Sci. Emerg. Technol.* **2014**, *26*, 366–374. [CrossRef]
10. Santonocito, D.; Raciti, G.; Campisi, A.; Sposito, G.; Panico, A.; Siciliano, E.A.; Sarpietro, M.; Damiani, E.; Puglia, C. Astaxanthin-loaded stealth lipid nanoparticles (AST-SSLN) as potential carriers for the treatment of alzheimer's disease: Formulation development and optimization. *Nanomaterials* **2021**, *11*, 391. [CrossRef]
11. Kumari, S.; Goyal, A.; Garg, M. Phytoconstituents Based Novel Nano-Formulations: An Approach. *ECS Transact.* **2022**, *107*, 7365. [CrossRef]
12. Hong, L.; Zhou, C.L.; Chen, F.P.; Han, D.; Wang, C.Y.; Li, J.X.; Chi, Z.; Liu, C.-G. Development of a carboxymethyl chitosan functionalized nanoemulsion formulation for increasing aqueous solubility, stability and skin permeability of astaxanthin using low-energy method. *J. Microencapsul.* **2017**, *34*, 707–721. [CrossRef] [PubMed]
13. Higuera-Ciapara, I.; Felix-Valenzuela, L.; Goycoolea, F.; Argüelles-Monal, W. Microencapsulation of astaxanthin in a chitosan matrix. *Carbohydr. Polym.* **2004**, *56*, 41–45. [CrossRef]
14. Feng, X.; Chen, A.; Zhang, Y.; Wang, J.; Shao, L.; Wei, L. Central nervous system toxicity of metallic nanoparticles. *Int. J. Nanomed.* **2015**, *10*, 4321.
15. Anarjan, N.; Tan, C.P.; Nehdi, I.A.; Ling, T.C. Colloidal astaxanthin: Preparation, characterisation and bioavailability evaluation. *Food Chem.* **2012**, *135*, 1303–1309. [CrossRef]
16. Garg, M.; Goyal, A.; Kumari, S. An Update on the Recent Advances in Cubosome: A Novel Drug Delivery System. *Curr. Drug Metab.* **2021**, *22*, 441–450. [CrossRef] [PubMed]
17. Almoshari, Y. Development, Therapeutic Evaluation and Theranostic Applications of Cubosomes on Cancers: An Updated Review. *Pharmaceuticals* **2022**, *14*, 600. [CrossRef]
18. Mathews, P.D.; Mertins, O.; Angelov, B.; Angelova, A. Cubosomal lipid nanoassemblies with pH-sensitive shells created by biopolymer complexes: A synchrotron SAXS study. *J. Colloid Interface Sci.* **2022**, *607*, 440–450. [CrossRef]
19. Bei, D.; Marszalek, J.; Youan, B.-B.C. Formulation of dacarbazine-loaded cubosomes—Part II: Influence of process parameters. *AAPS Pharm. Sci. Tech.* **2009**, *10*, 1040–1047. [CrossRef]
20. Kadawala, M.; Rao, L.; Sharma, L.; Sharma, V. Insights into the Recent Advancements in the Vibrant Area of Cubosomes Nanoparticles based Drug Delivery. *Int. J. Nanobiotech.* **2021**, *7*, 24–34.

21. Azman, K.A.K.; Seong, F.C.; Singh, G.K.S.; Affandi, M.M.R.M.M. Physicochemical characterization of astaxanthin-loaded PLGA formulation via nanoprecipitation technique. *J. Appl. Pharm. Sci.* **2021**, *11*, 05661.
22. Peng, X.; Zhou, Y.; Han, K.; Qin, L.; Dian, L.; Li, G.; Pan, X.; Wu, C. Characterization of cubosomes as a targeted and sustained transdermal delivery system for capsaicin. *Drug Des. Devel. Ther.* **2015**, *9*, 4209. [CrossRef] [PubMed]
23. Treuel, L.; Eslahian, K.; Docter, D.; Lang, T.; Zellner, R.; Nienhaus, K.; Nienhaus, G.U.; Stauber, R.H.; Maskos, M. Physicochemical characterization of nanoparticles and their behavior in the biological environment. *Phys. Chem. Chem* **2014**, *16*, 15053–15067. [CrossRef] [PubMed]
24. Weng, J.; Tong, H.H.; Chow, S.F. In vitro release study of the polymeric drug nanoparticles: Development and validation of a novel method. *Pharmaceuticals* **2020**, *12*, 732. [CrossRef]
25. Swami, H.; Bilandi, A.; Kataria, M.K.; Kaur, K. Formulation and evaluation of liposomal gel of lornoxicam. *World J. Pharm. Res.* **2015**, *4*, 2312–2338.
26. Singh, S.; Arora, S.; Allawadi, D. Formulation, optimization and evaluation of sustained release microspheres using Taguchi design. *J. Pharm. Technol. Res.* **2014**, *2*, 1–12. [CrossRef]
27. Eldeeb, A.E.; Salah, S.; Ghorab, M. Formulation and evaluation of cubosomes drug delivery system for treatment of glaucoma: Ex-vivo permeation and in-vivo pharmacodynamic study. *J. Drug Deliv. Sci. Technol.* **2019**, *52*, 236–247. [CrossRef]
28. Spicer, P.T.; Small, W.B.; Lynch, M.L.; Burns, J.L. Dry powder precursors of cubic liquid crystalline nanoparticles (cubosomes). *J. Nanopart. Res.* **2002**, *4*, 297–311. [CrossRef]
29. Rizwan, S.; Dong, Y.D.; Boyd, B.J.; Rades, T.; Hook, S. Characterisation of bicontinuous cubic liquid crystalline systems of phytantriol and water using cryo field emission scanning electron microscopy (cryo FESEM). *Micron* **2007**, *38*, 478–485. [CrossRef]
30. Shalaby, R.A.; El-Gazayerly, O.; Abdallah, M. Cubosomal Betamethasone-Salicylic Acid Nano Drug Delivery System for Enhanced Management of Scalp Psoriasis. *Int. J. Nanomed.* **2022**, *17*, 1659. [CrossRef]
31. Nasr, M.; Ghorab, M.K.; Abdelazem, A. In vitro and in vivo evaluation of cubosomes containing 5-fluorouracil for liver targeting. *Acta Pharm. Sin. B* **2015**, *5*, 79–88. [CrossRef] [PubMed]
32. Zhao, X.Y.; Zhang, J.; Zheng, L.Q.; Li, D.H. Studies of cubosomes as a sustained drug delivery system. *J. Dispers. Sci. Techn.* **2005**, *25*, 795–799. [CrossRef]
33. Singh, I.; Rana, V. Iron oxide induced enhancement of mucoadhesive potential of Eudragit RLPO: Formulation, evaluation and optimization of mucoadhesive drug delivery system. *Expert. Opin. Drug Deliv.* **2013**, *10*, 1179–1191. [CrossRef]
34. Baggi, R.B.; Kilaru, N.B. Calculation of predominant drug release mechanism using Peppas-Sahlin model, Part-I (substitution method): A linear regression approach. *Asian J. Pharm. Technol.* **2016**, *6*, 223–230. [CrossRef]
35. Prieto, J.M. Procedure: Preparation of DPPH Radical, and antioxidant scavenging assay. *DPPH Microplate Protoc.* **2012**, *2012*, 7–9.
36. Kurechi, T.; Kikugawa, K.; Kato, T. Studies on the antioxidants. XIII. Hydrogen donating capability of antioxidants to 2, 2-diphenyl-1-picrylhydrazyl. *Chem. Pharm. Bull* **1980**, *28*, 2089–2093.
37. Kaur, V.; Pawa, R.P. Formulation and evaluation of moxifloxacin hydrochloride niosomes for controlled ophthalmic drug delivery. *J. Pharm. Technol. Res. Manag.* **2015**, *3*, 11–28. [CrossRef]